12-pulse Rectifier with DC-Side Buck Converter for Electric Vehicle Fast Charging

Lan, Dun; Wu, Yang; Soeiro, Thiago Batista; Granello, Pierpaolo; Qin, Zian; Bauer, Pavol

DOI
10.1109/IECON49645.2022.9968872

Publication date
2022

Document Version
Final published version

Published in
IECON 2022 - 48th Annual Conference of the IEEE Industrial Electronics Society

12-pulse Rectifier with DC-Side Buck Converter for Electric Vehicle Fast Charging

Dun Lan
dept. DC Systems, Energy Conversion & Storage
Delft University of Technology
Delft, The Netherlands
D.Lan@student.tudelft.nl

Yang Wu
dept. DC Systems, Energy Conversion & Storage
Delft University of Technology
Delft, The Netherlands
Y.Wu-6@tudelft.nl

Thiago Batista Soeiro
dept. Power Management and Distribution Section (TEC-EPM)
European Space Agency
Noordwijk, The Netherlands
Thiago.BatistaSoeiro@esa.int

Pierpaolo Granello
dept. Astronautical, Electrical and Energetic Engineering
Sapienza University of Rome
Rome, Italy
pierpaolo.granello@uniroma1.it

Zian Qin
dept. DC Systems, Energy Conversion & Storage
Delft University of Technology
Delft, The Netherlands
Z.Qin-2@tudelft.nl

Pavol Bauer
dept. DC Systems, Energy Conversion & Storage
Delft University of Technology
Delft, The Netherlands
P.Bauer@tudelft.nl

IECON 2022 – 48th Annual Conference of the IEEE Industrial Electronics Society | 978-1-6654-8025-3/22/$31.00 ©2022 IEEE | DOI: 10.1109/IECON49645.2022.9968872

***Abstract*—This paper presents the study of a 100kW electric vehicle (EV) fast charger based on a 12-pulse rectifier cascaded with two buck-type DC-DC converters. The proposed circuit operates with a triangular current shaping method which considerably improves the current harmonics performance of the system. The studied circuit is particularly suited for high power battery charging, being relatively simple to operate, requiring a low active semiconductor count (only two active switches), and because it employs circuit technologies well-established in the high power market. Above all, this EV fast charger meets the requirements of isolation, high efficiency, high output voltage and good power quality (low THD and unity power factor). This paper describes in detail the analytical modeling of the studied circuit, including the current harmonic input filter design which meets the grid standard requirement, and the loss modeling of the semiconductors and passive elements. The modeling and simulation results of the proposed 100 kW system are presented and analyzed.**

***Index Terms*—EV fast charging, 12-pulse converter, Harmonic reduction, Triangular current shaping**

I. Introduction

With the growing interest and policy of electric vehicles (EV), EV share will have significant growth in the future, e.g., international energy agency (IEA) predicted the electric car share will be up to 14% in 2030 [1]. Charging problems and range concern have always been the main barriers of the EV market promotion [2]. The DC Fast charging technology can address well this problem and it is developing towards ultra-fast charging, which is capable of providing 150kW or more, expecting to charge EV battery to 80% within 10 minutes [6]. To charge a mainstream (e.g. Tesla Model S) 103kWh battery capacity to 80% in 10 minutes, the required fast charging power is 494.4 kW. The development of fast charging technology will therefore be of increasing importance to the EV development.

DC Fast charging systems (DCFCs) convert the AC voltage from the power grid to the DC voltage required for charging the EV batteries. There are several requirement from the application point of view, i.e., galvanic isolation for safety considerations, good power quality for the power grid and wide output voltage range for the flexible EV batteries available on the market. Besides, great efforts have been made to improve the converter efficiency and power density [3]. DCFCs can be designed as a single or a double converter stages [7]. The front-end converter for DCFCs can be divided into passive rectifiers (e.g.Multi-pulse rectifier) and active rectifiers (e.g.three-phase PWM rectifiers, such as the 2-level and 3-level neutral-point-clamped (NPC) or Vienna-type rectifiers) [8] [4]. The Multi-pulse rectifier (MPR) technology is widely used in high power application due to its simple structure, high robustness, and relatively low harmonic distortion [9]. Compared with active rectifier, Multi-pulse rectifier is simpler, more reliable but bulkier [10]. However, in high power applications the connection to the medium voltage (MV) distribution grid becomes important due to the power availability issues in the low voltage (LV) distribution grids. Therefore, a DCFC may naturally require a line frequency transformer to enable this MV grid connection, and the selection of the MPR technology can become a natural choice. Note that the required phase-shift transformer of the MPR already provides the required galvanic

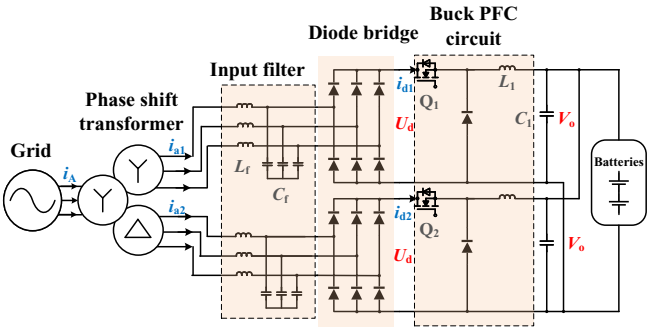

Fig. 1. DC fast battery charger based on the buck-type 12-pulse AC-DC converter.

isolation which is necessary for the EV charging, and hence, the usage of an extra isolated DC/DC conversion stage can be avoided. Overall, the Multi-pulse rectifier with an in-built power factor correction (PFC) functionality is very attractive for deriving a single converter stage fast EV battery charger.

Among the known MPRs, 12-pulse rectifier is the most widely used because of its economical and efficiency advantages [11]. One of the most effective harmonic reduction method for the 12-pulse converter is to shape the output current of two diode bridge to be close to a triangular shape by usage of auxiliary non-isolated DC-DC converter, which mostly implements a boost type circuit [10]. This kind of auxiliary circuit can be classified as current injection with interphase reactor (IPR) and separate modulation method [10]. Separate modulation method is simpler than the former one in terms of both the control and circuit realizations. In [12], the boost type separate modulation was implemented in a 12-pulse rectifier with the close to triangular current shaping method. A THDi of 3% was achieved but at the cost of considerable magnetic size. Another boost type 12-pulse rectifier with auto-transformer minimized the equivalent kVA rating of the transformer and improved the power density, but consequently resulted in a higher THD of 4.45%, which though is still in compliance with the IEEE519 standard [13]. Instead of the convention boost type circuit used in the literature, [14] proposed a full bridge type topology to meet isolation requirement while the losses increased significantly due to the larger part count of magnetic and semiconductor components.

In this article, a Buck type 12-pulse converter with triangular current shaping forthe DC fast battery charging application is designed and studied. This topology takes advantage of the high reliability and simplicity of the MPR, while also achieving low $\mathrm{THD_i}$ and high power factor on the AC side. For the application at hand, the selected buck-type PFC auxiliary circuit provides unique advantages over the boost type circuit previously used in the literature [15], namely: the natural current source functionality allows a direct connection to the battery, leading to much less DC filtering requirement; the solution can potentially enable direct start-up, while allowing for dynamic current limitation; and a wider output voltage control range, while maintaining PFC capability at the input. These advantages might result in the improvement of input power quality and efficiency of the system. Therefore, the buck-type 12-pulse converter featuring triangular current shaping is used for the 100 kW DC fast charger presented in this paper.

The rest of this paper is structured as follows. In section II, the 12-pulse buck type converter as well as the triangular current shaping method is introduced and the system are modelled. Section III presents the simulation results and analysis. In Section IV, experiment results are analyzed.

II. Proposed Buck-type 12-pulse Converter System

A. Topology of proposed converter

Fig. 1 shows the proposed topology of buck-type 12-pulse converter for the EV DC fast battery charging. A phase shift transformer with Y/Y/Δ connection provides galvanic isolation and the necessary 30 degree phase shift between each phase voltages delivered for the upper and lower diode bridges. An AC filter is necessary for grid-compliance, and two buck type DC-DC converter circuits use current and voltage control to separately control the output current of the two diode bridges to have a close to triangular shape which will provide the desired PFC capability and also to control the battery charging profile, e.g., the constant current (CC) and constant voltage (CV) battery charging.

B. Triangular Current Shaping Method for Harmonic Reduction

The turns ratio between the primary and the secondary windings in the star-star and star-delta transformers(Y/Y/Δ connection)is $1:k:\sqrt{3}k$. The input filter is a second order low pass filter which could have a small portion of the shunt capacitors, e.g., several 100 nF, moved to the output of the diode bridges in order to minimize the commutation loop of the buck type converter. As the cutoff frequency of the AC filter is tuned for attenuating the high-frequency components generated by the operation of the buck type converter, this doesn't influence the triangular current shaping method utilized in this work which has a relatively low frequency (e.g., 6x the grid frequency as shown in Fig. 2). Therefore, the influence of the AC filter to the low frequency components is omitted in the following analysis.

For the selected configuration of phase-shift transformer, the current relationship between the input phase current and the two diode bridge phase currents is expressed as

$$\begin{cases} k\cdot i_{\mathrm{A}} = i_{\mathrm{a1}} + (i_{\mathrm{a2}} - i_{\mathrm{b2}})/\sqrt{3} \\ k\cdot i_{\mathrm{B}} = i_{\mathrm{b1}} + (i_{\mathrm{b2}} - i_{\mathrm{c2}})/\sqrt{3} \\ k\cdot i_{\mathrm{C}} = i_{\mathrm{c1}} + (i_{\mathrm{c2}} - i_{\mathrm{a2}})/\sqrt{3} \end{cases} \tag{1}$$

$$\begin{cases} i_{\mathrm{a1}} = i_{\mathrm{d1}} S_{\mathrm{a1}}; i_{\mathrm{b1}} = i_{\mathrm{d1}} S_{\mathrm{b1}}; i_{\mathrm{c1}} = i_{\mathrm{d1}} S_{\mathrm{c1}}, \\ i_{\mathrm{a2}} = i_{\mathrm{d2}} S_{\mathrm{a2}}; i_{\mathrm{b2}} = i_{\mathrm{d2}} S_{\mathrm{b2}}; i_{\mathrm{c2}} = i_{\mathrm{d2}} S_{\mathrm{c2}}. \end{cases} \tag{2}$$

where $i_{\mathrm{A,B,C}}$ are the grid side phase currents, $i_{\mathrm{a1,b1,c1}}$ are the upper diode bridge phase currents, and $i_{\mathrm{a2,b2,c2}}$ are the lower diode bridge phase currents. i_{d1} and i_{d2} are the averaged output current of the two diode bridges. $S_{\mathrm{a1,b1,c1}}$ and $S_{\mathrm{a2,b2,c2}}$ are the

turn-on functions of each phase of the two diode bridge. S_{a1} can be expressed as

$$S_{\mathrm{a1}} = \begin{cases} 0 & \omega t \in \left[0, \frac{\pi}{6}\right] \\ 1 & \omega t \in \left[\frac{\pi}{6}, \frac{5\pi}{6}\right] \\ 0 & \omega t \in \left[\frac{5\pi}{6}, \frac{7\pi}{6}\right] \\ -1 & \omega t \in \left[\frac{7\pi}{6}, \frac{11\pi}{6}\right] \\ 0 & \omega t \in \left[\frac{7\pi}{6}, 2\pi\right] \end{cases} \tag{3}$$

Where ω is the angular grid frequency. The turn-on functions of the other phases (i.e. S_{b1},S_{b2} and so on) are of 120 degree phase shift relationship between different phases and 30 degree phase shift between the two diode bridges, which can be easily derived from S_{a1}.

The relationship between the input phase currents and the two diode bridge output currents is derived and can be expressed as

$$\begin{cases} k \cdot i_{\mathrm{A}} = A_1 i_{\mathrm{d1}} + A_2 i_{\mathrm{d2}} \\ k \cdot i_{\mathrm{B}} = B_1 i_{\mathrm{d1}} + B_2 i_{\mathrm{d2}} \\ k \cdot i_{\mathrm{C}} = C_1 i_{\mathrm{d1}} + C_2 i_{\mathrm{d2}} \end{cases} \tag{4}$$

where the coefficients A, B, and C are expressed as

$$\begin{cases} A_1 = S_{\mathrm{a1}} \\ A_2 = \left(S_{\mathrm{a2}} - S_{\mathrm{b2}}\right)/\sqrt{3} \\ B_1 = S_{\mathrm{b1}} \\ B_2 = \left(S_{\mathrm{b2}} - S_{\mathrm{c2}}\right)/\sqrt{3} \\ C_1 = S_{\mathrm{c1}} \\ C_2 = \left(S_{\mathrm{c2}} - S_{\mathrm{a2}}\right)/\sqrt{3} \end{cases} \tag{5}$$

The expected sinusoidal input phase current from the grid side is expressed as,

$$\begin{cases} i_{\mathrm{A}} = I \sin(\omega t) \\ i_{\mathrm{B}} = I \sin\left(\omega t - \frac{2\pi}{3}\right) \\ i_{\mathrm{C}} = I \sin\left(\omega t + \frac{2\pi}{3}\right) \end{cases} \tag{6}$$

where I is the amplitude of the AC grid current.

The averaged i_{d1} and i_{d2} from Eq. (4), (5) and (6), are expressed as (7) and shown in Fig. 2, where the transformer turns ratio k and current I are seen as reference values which depend on the local grid connection and power processed by the system.

$$\begin{cases} i_{\mathrm{d1}} = \frac{B_1 \sin(\omega t) - \frac{A_2}{B_2}\sin\left(\omega t - \frac{2\pi}{3}\right)}{A_1 - \frac{B_1}{B_2}A_2} k \cdot I \\ i_{\mathrm{d2}} = \frac{B_1 \sin(\omega t) - \frac{A_1}{B_1}\sin\left(\omega t - \frac{2\pi}{3}\right)}{A_2 - \frac{B_2}{B_1}A_1} k \cdot I \end{cases} \tag{7}$$

As shown in Fig. 2, i_{d1} and i_{d2} has $\pi/6$ phase shift and the shape of the current waveform is almost a standard triangular waveform. Noted that in reality the current waveform of the diode bridges is discontinuous formed by pieces of the impressed buck's inductor current. The averaged values derived in (7) and shown in Fig. 2 are the one derived after the AC filter.

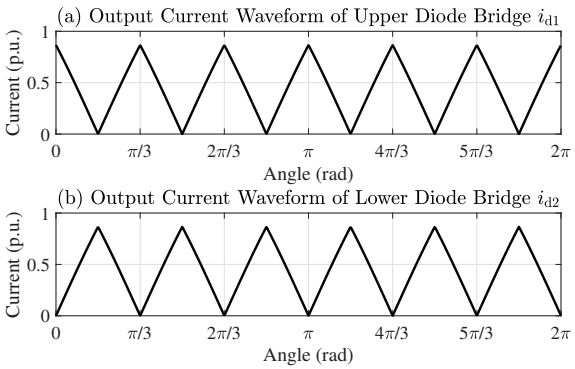

Fig. 2. Solved output current waveform of diode bridge from Eq. (7). Herein, $k = 1$ is considered and values are rated to the AC grid amplitude I.

C. System Parameter Design

As previously discussed the input current of the buck circuit is discontinuous, formed by the inductor current when the active semiconductor is turned On and null when the switch is turned Off. Therefor, the input filter is required to filter out the high frequency current component defined by the PWM operation of this DC-DC converter. The input filter, which in the studied case is a LC filter, can be designed as [16],

$$C_{\mathrm{f}} = \frac{D \cdot (1 - D) \cdot I_{\mathrm{o}}}{\Delta V_{C\mathrm{f}} \cdot f_{\mathrm{s}}} \tag{8}$$

$$L_{\mathrm{f}} = \frac{D \cdot (1 - D) \cdot I_{\mathrm{o}}}{8 \cdot \Delta I_{L\mathrm{f}} \cdot C_{\mathrm{f}} \cdot f_{\mathrm{s}}^2} \tag{9}$$

Note that the adding of the input filter will influence the stability margins of the feedback control loops of the buck circuit. For stability enhancement purpose, the use of passive or active damping technique at the input filter is advantageous. According to the Middlebrook's extra element theorem, adding the filter circuit to the buck converter will bring a correction factor M to the original transfer function. The control-to-output transfer function $G_{vd}(s)$ of the buck converter with input filter can be expressed as

$$G_{vd}(s)_{|Z_{\mathrm{o}}(s)=0} = \frac{V_{\mathrm{o}}(s)}{\hat{d}(s)} \tag{10}$$

$$G_{vd}(s) = \left(G_{vd}(s)_{|Z_{\mathrm{o}}(s)=0}\right) \cdot M \tag{11}$$

$$M(s) = \frac{1 + \frac{Z_{\mathrm{o}}(s)}{Z_{\mathrm{N}}(s)}}{1 + \frac{Z_{\mathrm{o}}(s)}{Z_{\mathrm{D}}(s)}} \tag{12}$$

$$Z_{\mathrm{D}}(s) = \frac{R}{D^2} \frac{1 + \frac{sL_1}{R} + s^2 L_1 C_1}{1 + sRC_1} \tag{13}$$

$$Z_{\mathrm{N}}(s) = -\frac{R}{D^2} \tag{14}$$

where $G_{vd}(s)_{|Z_{\mathrm{o}}(s)=0}$ is the control-to-output transfer function without input filter. $Z_{\mathrm{o}}(s)$ is the output impedance of the

input filter. $Z_{\mathrm{D}}(s)$ is the converter input impedance, with the controller variable $\hat{d}(s)$ set to zero, expressed as (13). $Z_{\mathrm{N}}(s)$ is the converter input impedance, with the output nulled to zero, expressed as (14). R is the equivalent load impedance modelled as a resistance.

For the stability of the buck control, the coefficient $M(s)$ should be close to 1. In case a passive damping circuit is used, to reduce the loss the damping resistor R_{f} could be paralleled connected with L_{f}. In this case the output impedance of the input filter $Z_{\mathrm{o}}(s)$ can be expressed as

$$Z_{\mathrm{o}}(s) = \frac{sR_{\mathrm{f}}L_{\mathrm{f}}}{s^2R_{\mathrm{f}}L_{\mathrm{f}}C_{\mathrm{f}} + sL_{\mathrm{f}} + R_{\mathrm{f}}} \tag{15}$$

The use of active damping or virtual resistance should be sought in the studied application in order to minimize the system losses. The input filter transfer function of the buck side current i_{B} to the grid side current i_{g} is expressed as

$$G_i(s) = \frac{i_{\mathrm{g}}}{i_{\mathrm{B}}} = \frac{sL_{\mathrm{f}} + R_{\mathrm{f}}}{s^2R_{\mathrm{f}}L_{\mathrm{f}}C_{\mathrm{f}} + sL_{\mathrm{f}} + R_{\mathrm{f}}} \tag{16}$$

The bode magnitude plot of the correction factor and input filter transfer function is shown in Fig. 3. Herein, the parameters of the input filter are set as $L_{\mathrm{f}} = 30\,\mu\mathrm{H}$, $C_{\mathrm{f}} = 15\,\mu\mathrm{F}$ and $R_{\mathrm{f}} = 5\,\Omega$.

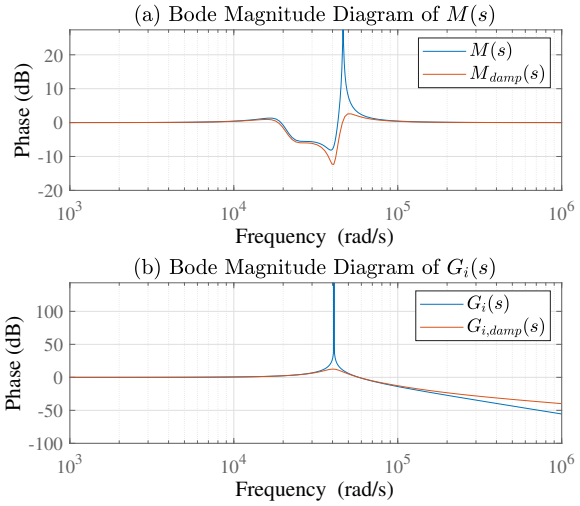

Fig. 3. Bode magnitude plot of $M(s)$ and $G_i(s)$

As it can be noted in Fig. 3, the utilization of damping provides great attenuation to oscillations at the resonance frequency of the filter, which make the system more robust to stability problems.

III. Simulation Results

A. Harmonic Distortion of the Input Current

Fig. 4 shows the input current waveform of phase A i_{A}, the secondary side current waveform of phase A i_{a1}, and the tertiary side current waveform of phase A i_{a1} and phase B i_{b2}. The transformer winding turns ratio k here is set to 1. As Fig. 4 shown, after the composition of the current component, the input current waveform is closed to sinusoidal. This demonstrates the feasibility of the triangular current shaping method with the buck converter circuit.

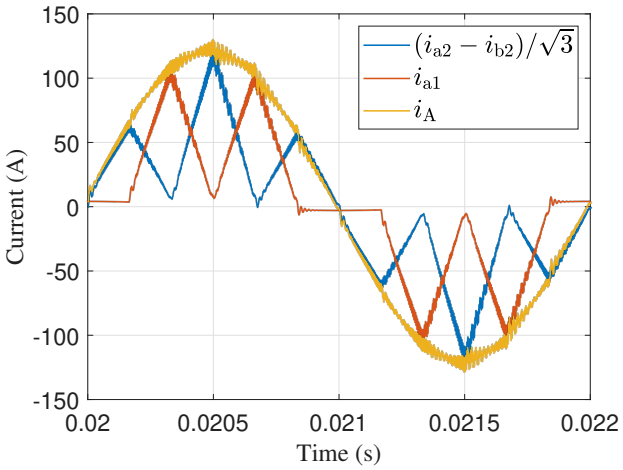

Fig. 4. Input current waveform.

The system is designed to meet the current harmonic limits of the IEEE 519-2014 standard. According to this standard [18], the recommended current distortion limits for systems nominally rated from 120 V up to 69 kV is of interest for this paper studied application.

From simulation result at full load (100 kW), the total harmonic distortion (THD) of the system, which is the same as the total demand distortion (TDD) under full load, is measured as 1.36% and conforms to the standard limits (5%). Power factor is measured as 0.999, which conforms to the standard (> 0.99). The individual harmonic order limits of the strictest standards $\frac{I_{\mathrm{SC}}}{I_{\mathrm{L}}} < 20$ and simulation result of the system are presented in Fig. 5. As Fig. 5 shown, all the simulated current harmonics conforms to the considered standard.

B. System Losses

Skin effect and proximity effect are considered in the calculation of the winding loss of the inductors and transformers. As the current is time-varying and non-sinusoidal, Improved Generalized Steinmetz Equation (IGSE) is used for calculating the core loss of the inductors and transformers [17]. SiC MOSFETs are selected as the switches to improve system efficiency [5]. Thus, reverse recovery losses of diodes could be ignored in the loss modelling.

Fig. 6 shows the proportion of losses of each part in the system with the setting of Table. I. In this setting, the system efficiency is 98.73%. The losses of the passive components L_1, L_{f} C_1 and C_{f} take 10% of the total loss. The losses of the Semiconductors (buck converter (33%) and rectifier diode bridges (23%)) take 56%, while the transformer contributes to 33 % of the total losses.

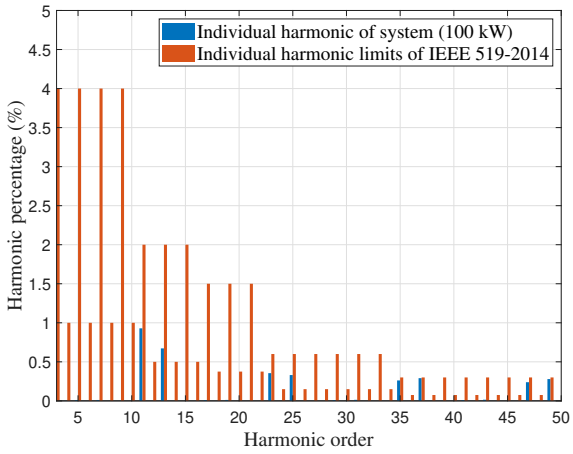

Fig. 5. Current individual harmonic distortion limits and system simulation result of $3 \leq h \leq 50$.

TABLE I
SYSTEM PARAMETERS

Parameters	Value	Unit
Grid Voltage (line-to-neutral)	220	V
Grid Frequency f_g	50	Hz
System output Power	100	kW
Transformer winding ratio k	1.8	
Switching Frequency of buck f_s	24	kHz
Output dc voltage V_o	800	V
Input Filter Inductor L_f	0.03	mH
Input Filter Capacitor C_f	15	μF
Input Filter Damping Resistor R_f	5	Ω
Buck Inductor L_1	0.1	mH
Buck Capacitor C_1	20	μF
Power Factor PF @ Full load	0.999	
THD$_i$ @ Full load	1.36	%
Efficiency η @ Full load	98.73	%
Diode Bridge	VUO52-16NO1	
SiC MOSFET	G3R2OMT17N	

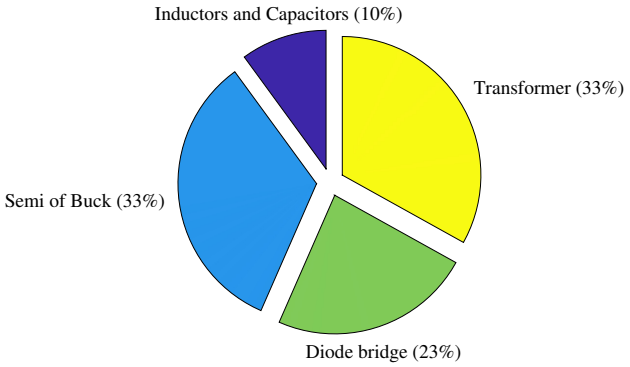

Fig. 6. The proportion of losses in each part of the system

IV. EXPERIMENT

In order to verify that the control strategy in buck circuit can control inductor current to keep track of the triangular current reference , a 1.7 kW six-pulse rectifier prototype was developed and analyzed in the laboratory, as shown in Fig. 7. Corresponding topology and control block are shown in Fig. 8. The setting parameters of the experiment set up are shown in Table. II.

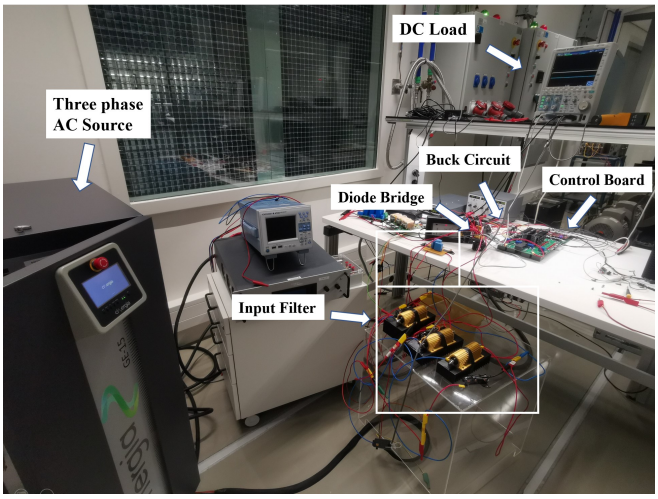

Fig. 7. Experimental setup overview

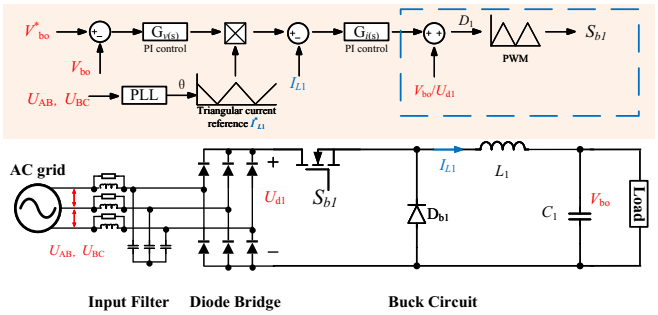

Fig. 8. Experimental setup topology and control scheme

TABLE II
PROTOTYPE PARAMETERS

Parameters	Value	Unit
Input Line Voltage	220	V_{rms}
DC Load as resistor	68	Ω
System output Power	1.7	kW
Switching Frequency f_s	36	kHz
Output dc voltage	300	V
Input Filter Inductor L_f	0.047	mH
Input Filter Capacitor C_f	4.7	μF
Input Filter Damping Resistor R_f	22	Ω
Buck Inductor L_1	0.1	mH
Buck Capacitor C_1	600	μF
Diode Bridge	VS-36MT160	
SiC MOSFET	IMW120R060M1	

The experiment results under close loop voltage and current control are shown in Fig. 9. In Fig. 9, the inductor current waveform of closed loop control could keep track of the triangular current reference and output voltage could be stable at 300V. This result verified that the voltage and current closed loop control work properly. The continuous current waveform of Phase A demonstrates that the input filter works properly as well.

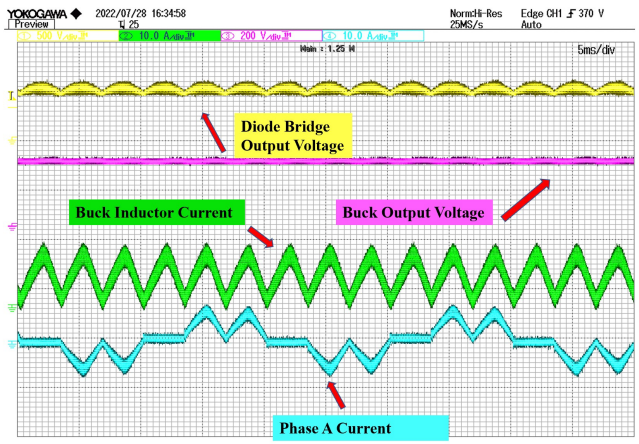

Fig. 9. Experimental results of voltage and current closed loop control

V. Conclusions

This paper presents an EV fast charging system based on a 12-pulse rectifier with buck type DC-DC converters. This uses a triangular current shaping method for current harmonic reduction. Even without isolated DC-DC converter stage, the system can also have a wide range of output voltage (between zero to the maximum voltage that system set at first). Besides, the system can maintain the grid input current to be sinusoidal with very low THD_i (1.36%) and high power factor (0.999), and conforms to the current harmonic limits of IEEE 519-2014. Moreover, the system has high efficiency (98.73%) for 800V output voltage. From the component point of view, fewer active components are used (only two MOSFETs) and lower inductance is needed, which reduces the losses and cost of the system. The galvanic isolation requirement is realized by a multi-pulse three phase transformer. Therefore, this system features a flexible high output voltage (tuned by the transformer turns ratio) and a wide range, high power quality, high efficiency and galvanic isolation, which allows it to be use as an EV fast charger.

References

[1] IEA (2021), Global EV Outlook 2021, IEA, Paris. https://www.iea.org/reports/global-ev-outlook-2021.

[2] S. Huang, B. Huang and F. Pai, "Fast Charge Strategy Based on the Characterization and Evaluation of LiFePO4 Batteries," in IEEE Transactions on Power Electronics, vol. 28, no. 4, pp. 1555-1562, April 2013.

[3] Xu, J., Soeiro, T. B., Wang, Y., Gao, F., Tang, H., Bauer, P. (2022). A Hybrid Modulation Featuring Two-phase Clamped Discontinuous PWM and Zero Voltage Switching for 99% Efficient DC-Type EV Charger. IEEE Transactions on Vehicular Technology, 71(2), 1454-1465. [9645178]. https://doi.org/10.1109/TVT.2021.3133647

[4] Xu, Junzhong, Gao, Fei, Batista, Thiago, Chen, Linglin, Tarisciotti, Luca, Tang, Houjun, Bauer, Pavol. (2020). Carrier-Based Modulated Model Predictive Control for Vienna Rectifiers. P.1-P.10. 10.23919/EPE20ECCEEurope43536.2020.9215826.

[5] J. Xu, J. Han, Y. Wang, M. Ali and H. Tang, "High-Frequency SiC Three-Phase VSIs With Common-Mode Voltage Reduction and Improved Performance Using Novel Tri-State PWM Method," in IEEE Transactions on Power Electronics, vol. 34, no. 2, pp. 1809-1822, Feb. 2019, doi: 10.1109/TPEL.2018.2829530.

[6] L. Wang, Z. Qin, T. Slangen, P. Bauer and T. van Wijk, "Grid Impact of Electric Vehicle Fast Charging Stations: Trends, Standards, Issues and Mitigation Measures - An Overview," in IEEE Open Journal of Power Electronics, vol. 2, pp. 56-74, 2021, doi: 10.1109/OJPEL.2021.3054601.

[7] H. Tu, H. Feng, S. Srdic and S. Lukic, "Extreme Fast Charging of Electric Vehicles: A Technology Overview," in IEEE Transactions on Transportation Electrification, vol. 5, no. 4, pp. 861-878, Dec. 2019.

[8] Khalid, M.R.; Khan, I.A.; Hameed, S.; Asghar, M.S.J.; Ro, J.-S. A Comprehensive Review on Structural Topologies, Power Levels, Energy Storage Systems, and Standards for Electric Vehicle Charging Stations and Their Impacts on Grid. IEEE Access 2021, 9, 128069–128094.

[9] S. P. P, R. Kalpana, B. Singh and G. Bhuvaneswari, "A 20-pulse asymmetric multiphase staggering autoconfigured transformer for power quality improvement", IEEE Trans. Power Electron., vol. 33, no. 2, pp. 917-925, Feb. 2018.

[10] Q. Du, L. Gao, Q. Li, T. Li and F. Meng, "Harmonic Reduction Methods at DC Side of Parallel-Connected Multipulse Rectifiers: A Review," in IEEE Transactions on Power Electronics, vol. 36, no. 3, pp. 2768-2782, March 2021.

[11] Fangang Meng, Wei Yang, Yi Zhu, Lei Gao and Shiyan Yang, "Load Adaptability of Active Harmonic Reduction for 12-Pulse Diode Bridge Rectifier With Active Interphase Reactor", IEEE Transactions on Power Electronics, vol. 30, no. 12, pp. 7170-7180, Dec. 2015.

[12] S. Choi, "A three-phase unity-power-factor diode rectifier," IEEE Trans. Ind. Electron., vol. 52, no. 6, pp. 1711–1714, Dec. 2005.

[13] Z. Liu, F. Meng and W. Yang, "Harmonic reduction technology at DC link in star-connected-autotransformer-based multi-pulse rectifier," 2017 IEEE Transportation Electrification Conference and Expo, Asia-Pacific (ITEC Asia-Pacific), 2017, pp. 1-6.

[14] S. Choi and Y. Bae, "A new unity power factor telecom rectifier system by an active waveshaping technique," in Proc. Conf. Rec. IAS Annu. Meeting, 2005, pp. 917–922.

[15] T. B. Soeiro, M. L. Heldwein and J. W. Kolar, "Three-phase modular multilevel current source rectifiers for electric vehicle battery charging systems," 2013 Brazilian Power Electronics Conference, 2013, pp. 623-629, doi: 10.1109/COBEP.2013.6785180.

[16] K. Ejjabraoui, C. Larouci, P. Lefranc and C. Marchand, "Pre-sizing methodology of dc-dc converters using optimization under multi-phySiC constraints; Application to a buck converter," IEEE Trans. on Industrial Electronics; Vol.59, No.7, pp. 2781 - 2790, 2012.

[17] K. Venkatachalam, C. R. Sullivan, T. Abdallah and H. Tacca, "Accurate prediction of ferrite core loss with nonsinusoidal waveforms using only Steinmetz parameters," 2002 IEEE Workshop on Computers in Power Electronics, 2002. Proceedings., 2002, pp. 36-41, doi: 10.1109/CIPE.2002.1196712.

[18] "IEEE Recommended Practice and Requirements for Harmonic Control in Electric Power Systems," in IEEE Std 519-2014 (Revision of IEEE Std 519-1992) , vol., no., pp.1-29, 11 June 2014.